

Separating the Mechanisms of Transient Responses to Stratospheric Ozone Depletion–Like Cooling in an Idealized Atmospheric Model

HUANG YANG

Department of Earth and Atmospheric Sciences, Cornell University, Ithaca, New York

LANTAO SUN

National Center for Atmospheric Research, Boulder, Colorado*

GANG CHEN

Department of Earth and Atmospheric Sciences, Cornell University, Ithaca, New York

(Manuscript received 6 November 2013, in final form 7 October 2014)

ABSTRACT

Previous studies have suggested that Southern Hemisphere (SH) summertime trends in the atmospheric circulation in the second half of the twentieth century are mainly driven by stratospheric ozone depletion in spring. Here, the authors show that the pattern and timing of observed trends, characterized by downward propagation of signals, can be approximately captured in an idealized atmospheric global circulation model (AGCM) by imposing ozone depletion–like radiative cooling.

It is further shown that the synoptic eddies dominantly contribute to the transient tropospheric response to polar stratospheric cooling. The authors examine three possible mechanisms on the downward influence of polar stratospheric cooling. The polar stratospheric cooling affects tropospheric synoptic eddies via (i) the direct influences on the lower-stratospheric synoptic eddies, (ii) the planetary wave–induced residual circulation, and (iii) the planetary eddy–synoptic eddy nonlinear interaction. It is argued that the planetary wave–induced residual circulation is not the dominant mechanism and that the planetary eddies and further nonlinear interaction with synoptic eddies are more likely the key to the downward influence of the ozone depletion–like cooling.

1. Introduction

Substantial evidence has suggested that the Southern Hemisphere (SH) summertime circulation trends over the late twentieth century are primarily caused by the anthropogenic Antarctic ozone hole in spring [see [Polvani et al. \(2011\)](#), and references therein]. These circulation changes are characterized by a strengthening of the circumpolar winds in the lower stratosphere, an accelerated polar downwelling in the stratosphere ([McLandress et al. 2010](#);

[Lin and Fu 2013](#)), and a trend toward the positive phase of the southern annular mode (SAM) in the troposphere associated with a poleward shift of the tropospheric eddy-driven jet [see the review by [Thompson et al. \(2011\)](#)].

Given the complex interplay between chemistry, radiation, and dynamics in the tropospheric response to stratospheric ozone depletion, the underlying mechanism(s) has (have) not been fully understood ([Thompson et al. 2011](#)). By directly imposing stratospheric ozone loss, [Orr et al. \(2012\)](#) found the feedback between the upward cross-tropopause propagation of planetary waves and the strength of the stratospheric polar vortex is crucial to explain the downward influence of the ozone depletion radiative cooling on the tropospheric jet shift. In an idealized model, [Kushner and Polvani \(2004](#), hereafter [KP04](#)) showed that the tropospheric jet moves poleward in response to idealized polar stratospheric cooling and emphasized the importance of eddies. Using a similar

* The National Center for Atmospheric Research is sponsored by the National Science Foundation.

Corresponding author address: Huang Yang, Department of Earth and Atmospheric Sciences, Cornell University, Ithaca, NY 14853.
E-mail: hy337@cornell.edu

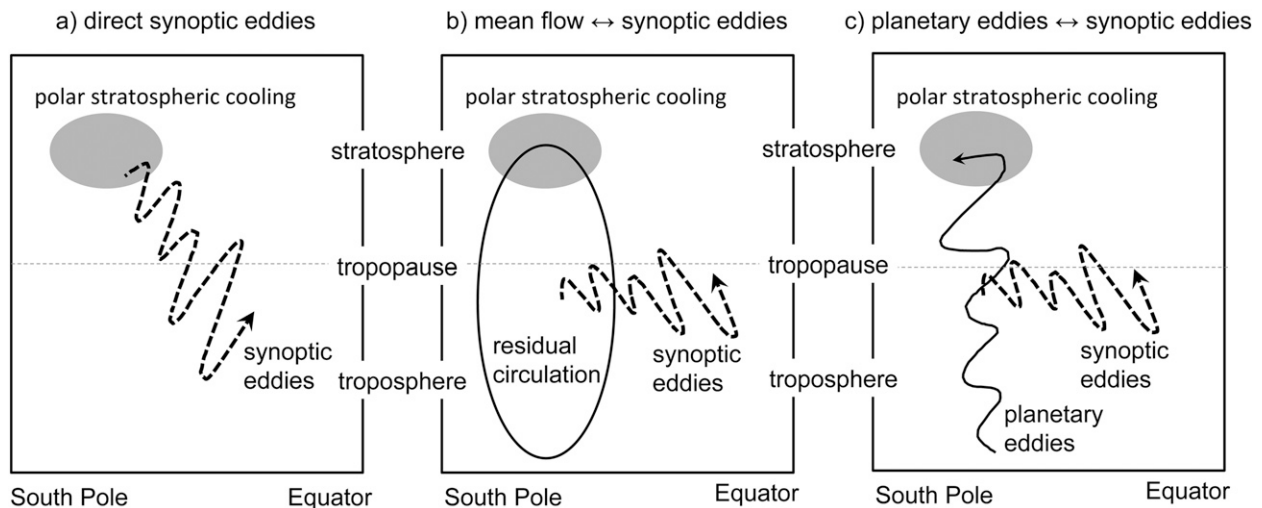


FIG. 1. Mechanisms by which ozone depletion–like stratospheric cooling impacts synoptic eddies: (a) the stratospheric radiative cooling induces a direct impact on synoptic eddies; (b) the stratospheric radiative cooling generates planetary wave drag anomalies, and a planetary wave–induced residual circulation impacts synoptic eddies by the anomalous zonal flow associated with the residual circulation; and (c) the stratospheric radiative cooling impacts the planetary waves in the stratosphere and troposphere via changes in reflection and propagation, and altered planetary waves then interact with the synoptic eddies by nonlinear eddy–eddy interactions.

model, [Song and Robinson \(2004\)](#) found that the tropospheric response to stratospheric forcing is largely reduced when planetary waves are damped. Recently, [Sun et al. \(2014\)](#) stressed that the delay in the breakdown of the polar vortex is crucial in producing a deep response in planetary waves that can, in turn, influence the tropospheric circulation.

It is then important to understand how the stratospheric perturbation from ozone depletion can impact the synoptic waves in the troposphere that dominate the tropospheric variability. Three mechanisms are illustrated schematically in [Fig. 1](#). First, the radiative cooling from the ozone depletion can directly influence the synoptic eddies in the upper troposphere and lower stratosphere via increased tropopause height ([Williams 2006](#); [Lorenz and DeWeaver 2007](#); [Simpson et al. 2009](#)) or accelerated synoptic eddy phase speed ([Wittman et al. 2007](#); [Chen and Held 2007](#)). Through interactions with the zonal flow, these synoptic eddy anomalies in the lower stratosphere can further communicate with the tropospheric synoptic eddies. Second, the radiative cooling can produce a stratospheric planetary wave change, and this anomalous planetary wave drag can induce a residual-mean meridional circulation that extends downward into the troposphere, as described by the downward control mechanism ([Haynes et al. 1991](#)). In the troposphere, a weak zonal flow anomaly associated with the residual circulation can be amplified by a positive synoptic eddy feedback (e.g., [Lorenz and Hartmann 2001](#)). This was summarized as the downward control with eddy feedback (DCWEF) mechanism by [Song and Robinson \(2004\)](#),

who found a more poleward tropospheric jet when an eastward zonal torque is applied to the polar stratosphere. Last, the stratospheric zonal flow anomalies, initiated by the ozone depletion radiative cooling, can impact planetary eddies through wave propagation ([Chen and Robinson 1992](#)) and wave refraction ([Shaw et al. 2010](#)). While propagating downward, the changes in planetary eddies can directly couple with synoptic eddies via nonlinear eddy–eddy interaction to produce a pronounced tropospheric response.

Although most previous studies have focused on the tropospheric responses to stratospheric perturbations in the winter solstice, idealized models can also simulate qualitatively the seasonal cycle in the Brewer–Dobson circulation (BDC) from winter to summer ([Chen and Sun 2011](#)) and the final breakdown of the polar vortex in spring ([Sun and Robinson 2009](#); [Sun et al. 2011](#)). [Sun et al. \(2014\)](#) used the idealized model of KP04 to simulate the pattern and timing of the observed trends in austral summer by applying idealized radiative cooling to the polar stratosphere in spring. They found the timing of the stratospheric polar vortex breakdown and planetary wave drag is critical for the tropospheric response. Specifically, while the synoptic eddies can interact with the polar stratospheric cooling in both delayed stratospheric final warming (SFW) and undelayed SFW events, only the composite from the years with delayed SFW has a strong tropospheric circulation response, accompanied by distinct behaviors of the lower-stratosphere temperature anomalies and planetary eddies (see their Figs. 10 and 11, respectively). This

indicates that both the radiative cooling and the eddies can be crucial in interpreting the downward influence of stratospheric ozone depletion–like cooling toward tropospheric circulation. As such, in this work, we will further separate the mechanisms of transient circulation responses simulated in this model (Sun et al. 2014).

The paper is organized as follows. Section 2 introduces the diagnostics in a quasigeostrophic framework to separate the wind tendency into contributions from polar stratospheric cooling and eddy forcings. The idealized model of the atmosphere used in this study is described in section 3. In section 4, we present the analysis of the transient circulation responses to stratospheric ozone depletion–like cooling. Conclusions are given in section 5. Details of the zonally symmetric model are summarized in the appendix.

2. Diagnostics in a quasigeostrophic framework

For simplicity, we introduce the diagnostics using a quasigeostrophic (QG) framework. Following Eq. (3.5.7) in Andrews et al. (1987), the zonal wind tendency can be written as

$$\begin{aligned} \mathcal{L}\left(\frac{\partial \bar{u}}{\partial t}\right) &\equiv \left[\frac{\partial^2}{\partial y^2} + \frac{1}{\rho_0} \frac{\partial}{\partial z} \left(\rho_0 \frac{f_0^2}{N^2} \frac{\partial}{\partial z} \right) \right] \frac{\partial \bar{u}}{\partial t} \\ &= \frac{\partial^2}{\partial y^2} \left(\frac{1}{\rho_0} \nabla \cdot F + \bar{X} \right) - \frac{1}{\rho_0} \frac{\partial^2}{\partial z \partial y} \left(\frac{\rho_0 f_0 \bar{\mathcal{H}}}{d\theta_0/dz} \right), \end{aligned} \tag{1}$$

where $\mathcal{L}(X) = \partial^2 X / \partial y^2 + (1/\rho_0)(\partial/\partial z)[\rho_0(f_0^2/N^2)(\partial X/\partial z)]$ is a linear elliptic operator and its inversion $\mathcal{L}^{-1}(X)$ can be nonlocal, $\rho_0(z) \propto e^{-z/H}$, $N^2(z) = (g/\theta_0)(d\theta_0/dz)$, $\nabla \cdot F$ denotes the Eliassen–Palm flux divergence, \bar{X} denotes momentum forcing (i.e., surface friction and unresolved wave drag), $\bar{\mathcal{H}}$ denotes diabatic heating, and readers are referred to Andrews et al. (1987) for conventions of other symbols. Given appropriate boundary conditions, the zonal wind tendency can be attributed linearly through the inverted operator \mathcal{L}^{-1} to the eddy forcing, momentum forcing, and diabatic heating, respectively. The nonlocal response takes place through altered residual overturning circulations that are implicit in the operator.

Using the radiative cooling rate from ozone depletion Q , we can obtain the tendency of the anomalous zonal wind $\delta \bar{u}$ as

$$\frac{\partial \delta \bar{u}^Q}{\partial t} = -\mathcal{L}^{-1} \left[\frac{1}{\rho_0} \frac{\partial^2}{\partial z \partial y} \left(\frac{\rho_0 f_0 \bar{Q}}{d\theta_0/dz} \right) \right]. \tag{2}$$

Similarly, we can obtain the anomalous zonal wind tendencies due to the changes of planetary wave forcing δF^p and synoptic eddy forcing δF^s as

$$\frac{\partial \delta \bar{u}^p}{\partial t} = \mathcal{L}^{-1} \left[\frac{\partial^2}{\partial y^2} \left(\frac{1}{\rho_0} \nabla \cdot \delta F^p \right) \right] \quad \text{and} \tag{3}$$

$$\frac{\partial \delta \bar{u}^s}{\partial t} = \mathcal{L}^{-1} \left[\frac{\partial^2}{\partial y^2} \left(\frac{1}{\rho_0} \nabla \cdot \delta F^s \right) \right]. \tag{4}$$

The total zonal wind response to radiative cooling and eddy forcings can be obtained as $\delta \bar{u} = \delta \bar{u}^Q + \delta \bar{u}^p + \delta \bar{u}^s$.

For the second mechanism shown in Fig. 1b, the polar stratospheric cooling and planetary wave forcing can induce a zonal wind change via the residual circulations, as diagnosed from $\delta \bar{u}^Q + \delta \bar{u}^p$ (note that this includes planetary waves in both the stratosphere and troposphere). As synoptic eddies can provide a positive feedback to the zonal jet variability (e.g., Lorenz and Hartmann 2001), the positive feedback is expected to maintain or amplify the zonal jet shift that is diagnosed from $\delta \bar{u}^Q + \delta \bar{u}^p$. On the other hand, as shown in Fig. 1c, stratospheric cooling and the resultant polar vortex change may alter planetary wave propagation (Chen and Robinson 1992) and reflection (Shaw et al. 2010) in the vertical direction. The change in planetary waves may impact synoptic eddies directly via nonlinear eddy–eddy interactions.

It should be noted that boundary conditions are crucial for the diagnostics in the QG framework (Haynes and Shepherd 1989). To avoid this problem, we have used the same idealized model (described in section 3) to construct a zonally symmetric model with the same boundary conditions. Also, eddy forcings are computed directly within the same model (described in the appendix) to be consistent with the model discretization in the horizontal and vertical directions.

3. Model setup

We use the Geophysical Fluid Dynamics Laboratory (GFDL) atmospheric dynamical core at T42 horizontal resolution and 40 unevenly spaced sigma levels. Following Kushner and Polvani (2006), the control simulation is forced by a Newtonian relaxation toward a prescribed time-dependent zonally symmetric radiative equilibrium temperature profile T_{eq} and damped by a linear friction in the planetary boundary layer. As illustrated by contours in Fig. 2, T_{eq} in the polar stratosphere is set by the lapse rate $\gamma = 6 \text{ K km}^{-1}$ in midwinter and $\gamma = 0 \text{ K km}^{-1}$ in midsummer, and the variation between midwinter and midsummer induces a stratospheric seasonal cycle [here γ is defined as in Eq. (3) of KP04]. The value of T_{eq} in the troposphere, on the other hand, is set by a hemispheric asymmetry parameter $\epsilon = 10 \text{ K}$ to yield perpetual austral summer. This setup ensures that the downward influence of SFWs in the troposphere is initialized from the stratosphere. Moreover,

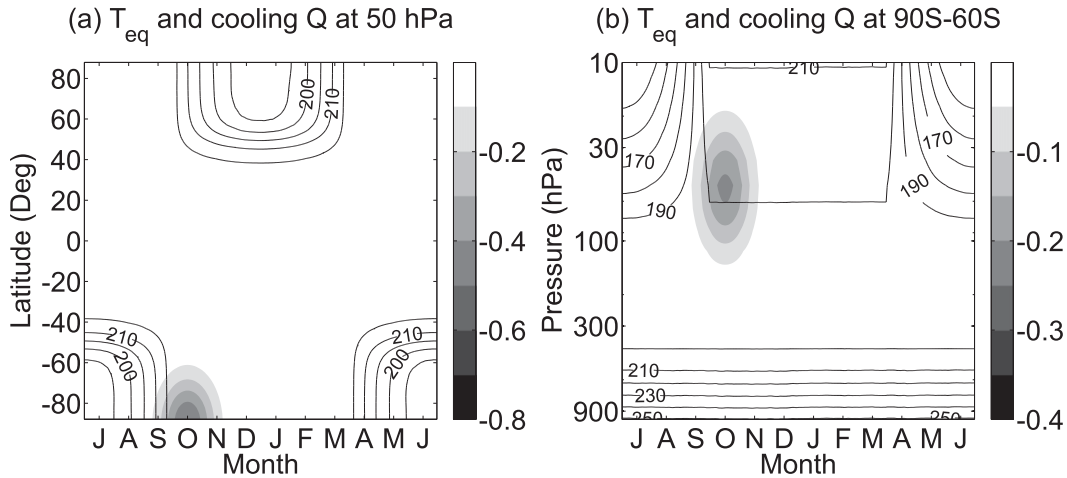


FIG. 2. The annual cycle of the equilibrium temperature profile (contours interval: 5 K) in the control run and additional ozone depletion–like radiative cooling in the perturbation run (shading; K day^{-1}). (a) The meridional distribution at 50 hPa and (b) vertical distribution averaged over the polar cap ($90^\circ\text{--}60^\circ\text{S}$).

there is no topography, but planetary waves can be generated through nonlinear interactions of baroclinic waves (Scinocca and Haynes 1998).

In the perturbation run, following Sun et al. (2014), radiative cooling induced by stratospheric ozone depletion is mimicked by idealized polar stratospheric cooling in spring as

$$Q(\phi, \sigma, t) = (0.5 \text{ K day}^{-1}) \times \exp \left\{ - \left[\frac{(\phi - \phi_0)^2}{2\sigma_\phi^2} + \frac{(-7000 \ln \sigma + 7000 \ln \sigma_0)^2}{2\sigma_\sigma^2} + \frac{(t - t_0)^2}{2\sigma_t^2} \right] \right\}. \quad (5)$$

Here the parameters $\phi_0 = -1.57$, $\sigma_\phi = 0.28$, $\sigma_0 = 0.05$, and $\sigma_\sigma = 4000$ (where ϕ denotes the latitude, the sigma level $\sigma = p/p_s$, p is the pressure, and p_s is the surface pressure) define the spatial pattern of cooling [similar to Butler et al. (2010)]. The time t_0 (corresponds to 1 October), $\sigma_t = 20$ days, and the time t define the peak and persistence of cooling, respectively. The pattern of cooling is shown by shading in Fig. 2, which mimic the observed structure of the Antarctic ozone hole [e.g., Fig. 1 in Polvani et al. (2011)]. As such, we have assumed that the polar stratospheric cooling in observations is dominated by the radiative cooling due to the ozone depletion, although our simulations can also produce small dynamical cooling due to the residual circulation anomalies driven by altered wave forcing in the presence of anomalous radiative cooling (Figs. 4g,i).

The control run (FM_C) is integrated for 80 years after a year of spinup is discarded. Starting from the beginning of austral autumn each year, a 1-yr time-slice experiment is

performed with the polar stratospheric cooling [Eq. (5)] turned on in the spring to form an 80-yr ensemble of perturbed run (FM_F). A brief summary of the numerical experiments and notations of experiments are described in Table 1. The perturbed run minus the control run is referred to as the ozone depletion response (i.e., $\text{FM}_F - \text{FM}_C$).

To assess the effects of planetary eddies and synoptic eddies in the downward influence of polar stratospheric cooling on the tropospheric circulation, a zonally symmetric model is constructed, as in KP04. With only zonal-mean quantities being resolved, the zonally symmetric model is unable to simulate eddy forcings directly. The eddy effect on the zonal-mean flow can be assessed by adding the eddy forcings extracted from the full model (i.e., FM_F) as external forcings to the zonally symmetric model for integration of the zonal means of zonal wind, meridional wind, temperature, and surface pressure, respectively. Unlike KP04 who used the time-mean eddy forcings, here we have calculated 80-yr-mean annual cycles of eddy forcings in the full model (i.e., FM_F) to drive the zonally symmetric model (see the appendix for details).

As illustrated in the QG framework in section 2, the transient ozone depletion responses (i.e., $\text{FM}_F - \text{FM}_C$) can be separated by individual responses to radiative cooling with no eddy forcing, planetary eddy changes alone (zonal wavenumbers 1–3), and synoptic eddy changes alone (zonal wavenumbers 4 and above). These three perturbation simulations minus the corresponding control run in the zonally symmetric model are separately referred to as radiative cooling, planetary eddy, and synoptic eddy responses (i.e., $\text{ZM}_Q - \text{ZM}_C$, $\text{ZM}_P - \text{ZM}_C$, and $\text{ZM}_S - \text{ZM}_C$). Furthermore, the zonally symmetric model simulation with all these three forcings included (i.e., $\text{ZM}_F - \text{ZM}_C$) successfully reproduces the ozone depletion

TABLE 1. Summary of numerical experiments. “Resolved” denotes that the component is resolved in the model. “Specified” denotes that the component is specified using Eq. (A4) and the simulation indicated in the parentheses. See the text in section 3 and the appendix for details.

Model	Expt	Description	Zonal means	Planetary eddies	Synoptic eddies	Ozone loss
Full model	FM _C	Control	Resolved	Resolved	Resolved	No
	FM _F	Forced ozone depletion	Resolved	Resolved	Resolved	Yes
	FM _P	Planetary eddy	Resolved	Resolved plus specified anomaly (FM _F – FM _C)	Resolved	No
Zonally symmetric model	ZM _C	Control	Resolved	Specified (FM _C)	Specified (FM _C)	No
	ZM _F	Total forcing	Resolved	Specified (FM _F)	Specified (FM _F)	Yes
	ZM _O	Radiative cooling	Resolved	Specified (FM _C)	Specified (FM _C)	Yes
	ZM _P	Planetary eddy	Resolved	Specified (FM _F)	Specified (FM _C)	No
Synoptic wave model	ZM _S	Synoptic eddy	Resolved	Specified (FM _C)	Specified (FM _F)	No
	SM _C	Control	Resolved	Specified (FM _C)	Resolved	No

responses in the full model (i.e., FM_F – FM_C, cf. the full model in Figs. 3d–f and the zonally symmetric model in Figs. 4a–c).

4. Results

We first compare the transient responses to polar stratospheric cooling simulated in the idealized model with the observed trends in the Interim European Centre

for Medium-Range Weather Forecasts (ECMWF) Re-analysis (ERA-Interim; Dee et al. 2011) (Fig. 3). The observed trends are calculated with a linear trend for the years 1979–2002 and the months of September–February, when pronounced ozone depletion has developed in the stratosphere followed by tropospheric signals (e.g., Thompson et al. 2011).

Despite its simplicity, the idealized model can capture many important features of the observed trends in the

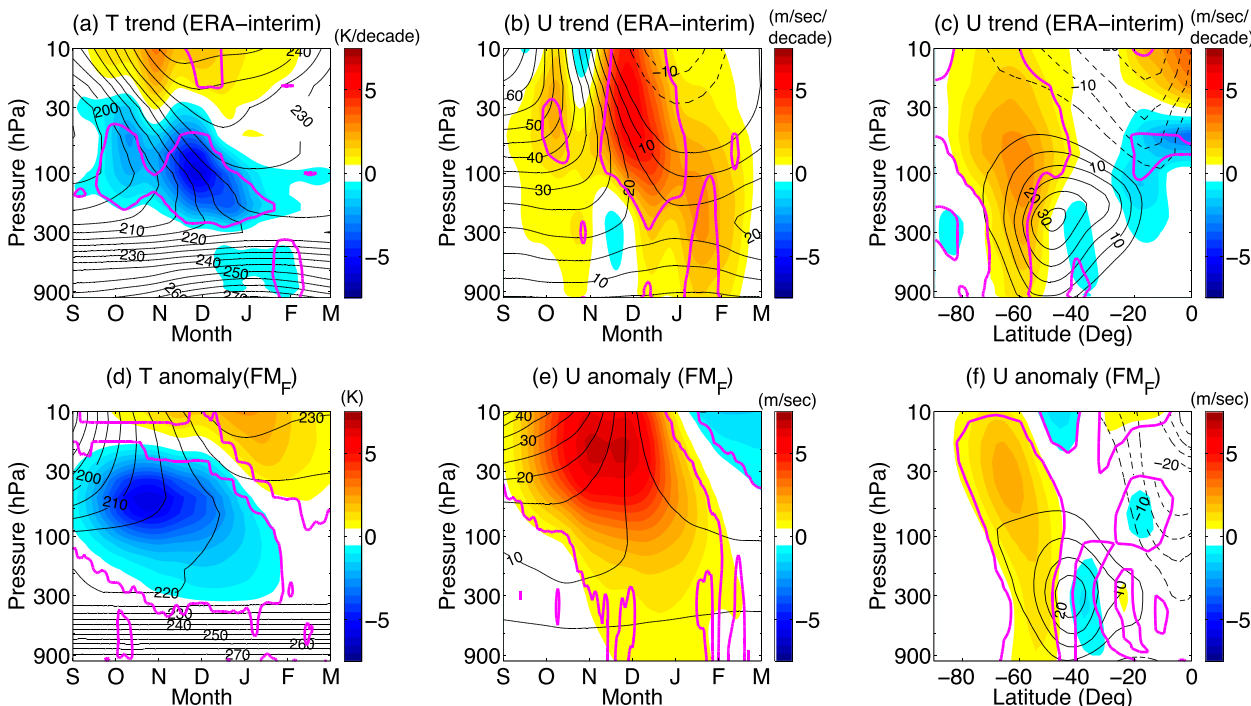


FIG. 3. Comparison between (a)–(c) ERA-interim and (d)–(f) the idealized full model with ozone depletion-like cooling. (a),(d) The temporal variation of zonal-mean temperature over the polar cap (averaged over 90°–60°S); (b),(e) the temporal variation of zonal-mean zonal winds at the edge of the polar cap (averaged over 70°–50°S); and (c),(f) latitude–altitude cross section of zonal-mean zonal winds during the austral summer (DJF). Climatologies are shown as contours (solid for positive values and dashed for negative). Shades denote the trends over 1979–2002 (K decade^{−1} for temperature or m sec^{−1} decade^{−1} for zonal wind) in the ERA-Interim and the anomalies (K for temperature or m sec^{−1} for zonal wind) in the idealized model simulation. The signals in regions enclosed by purple contours are significant above the 95% confidence level using a two-sided Student’s *t* test.

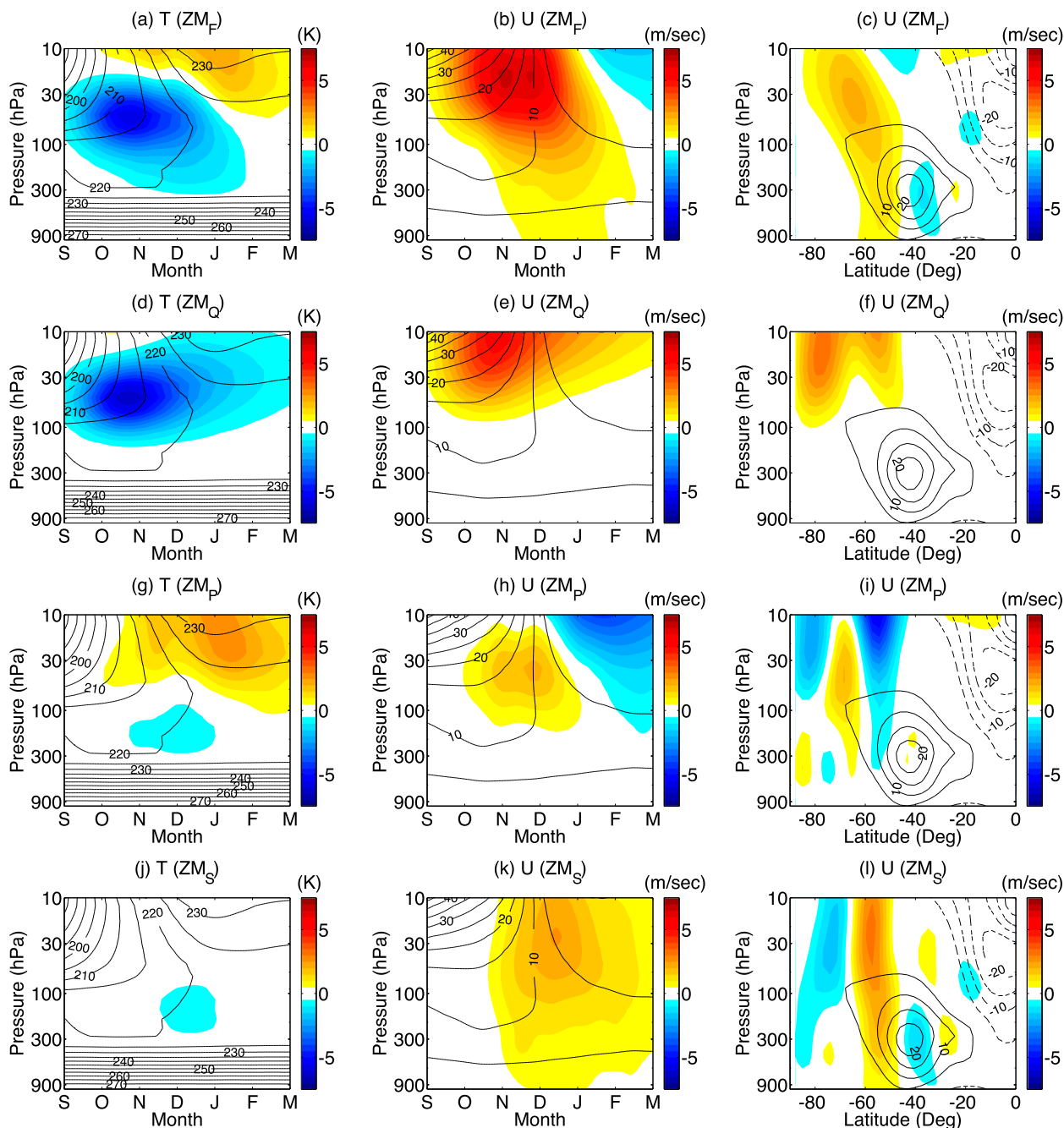


FIG. 4. As in Fig. 3d–f, but for the anomalies in the zonally symmetric model separated by individual forcings: (a)–(c) with total forcing, (d)–(f) with spring-cooling forcing only, (g)–(i) with planetary eddy forcing only, and (j)–(l) with synoptic eddy forcing only. See the text in section 3 for details.

reanalysis data. In the polar region (90° – 60° S), the temperature is cooled, as expected, in spring between 30 and 300 hPa; this cooling migrates downward with dynamical warming aloft (Figs. 3a,d). There is anomalous westerly wind at the edge of the polar vortex (70° – 50° S) in early summer, indicating a delayed breakdown of the polar vortex (Figs. 3b,e). The westerly anomaly

propagates from the stratosphere to the troposphere. To highlight the structure of tropospheric wind change, the zonal wind response in December–February (DJF) is plotted in the latitude–altitude cross section (Figs. 3c,f). The tropospheric wind is characterized as a poleward shift of the tropospheric jet that projects positively onto the SAM. The similarities between the reanalysis data

and the idealized model indicate that the polar stratospheric cooling induced by ozone depletion alone can contribute to the surface wind trends in observations, as in the idealized model.

There are also noticeable differences between the idealized model and observations. The seasonal transition of stratospheric anomalies in the model is more gradual than the observed trends, which may be attributed to the simplicity of idealized ozone depletion cooling. In the idealized model, the maximum tropospheric zonal wind anomalies occur right after the corresponding maximum stratospheric anomalies in early summer (cf. Fig. 3e), while, in the observations, the tropospheric maximum occurs in midsummer with a distinct lag from its stratospheric counterpart. Also, the tropospheric zonal wind anomalies are more equatorward in the model than observations, which may be explained by an equatorward bias in the climatological jet. Despite these shortcomings, the model provides a simple framework to understand, at least qualitatively, the mechanism(s) of the tropospheric response to stratospheric ozone loss.

Using the zonally symmetric model, we can separate the mechanisms of transient tropospheric response to individual forcings, as noted in sections 2 and 3. Figure 4 shows a separation of atmospheric ozone depletion responses discussed above into contributions from radiative cooling, planetary waves, and synoptic waves. We find, as expected, that the lower stratospheric cooling initially in spring is dominated by prescribed radiative cooling. As the polar cooling without any eddy forcing tends to migrate upward as time evolves (Fig. 4d), the downward migration seen in the full model (i.e., $FM_F - FM_C$) should be attributed to the change in eddy forcing, consistent with Orr et al. (2013). Particularly, the mid-stratosphere warming in late spring and summer (Fig. 4g) is dynamically driven by the polar downwelling (not shown) associated with enhanced planetary wave drags. This is consistent with the strengthened polar downwelling of the BDC in summer simulated in chemistry–climate models with realistic ozone depletion (McLandress et al. 2010; Lin and Fu 2013; Orr et al. 2013).

The change in subpolar zonal wind is consistent with polar cap temperature by the thermal wind relationship. Without any eddy forcing, the springtime strengthening of the polar vortex remains above the level of thermal forcing (Fig. 4e). It is therefore the eddy forcing that drives the downward propagation of westerly anomalies from the stratosphere into the troposphere. In response to planetary wave forcing, the polar stratospheric wind is strengthened in late spring and weakened in summer (Fig. 4h), which indicates a delay in the breakdown of polar vortex and planetary wave drag, as found in

McLandress et al. (2010) and Sun et al. (2014). For the downward propagation of anomalous westerlies, planetary waves and synoptic waves in early summer work constructively in the stratosphere, and synoptic waves are the primary driver of the tropospheric signal. The increased planetary wave drag in late summer (not shown) causes anomalous stratospheric easterlies in the full model (i.e., $FM_F - FM_C$). While most synoptic waves are confined in the troposphere, synoptic waves drive persistent anomalous westerlies from the surface to the stratosphere throughout the summer (Fig. 4k, also seen in Fig. 4l and discussed later).

As for the meridional structure of zonal wind in austral summer (DJF), spring cooling with no eddy forcing can induce a zonal wind increase only in the polar stratosphere (Fig. 4f). By contrast, planetary waves lead to the zonal wind deceleration at 50° – 60° S and acceleration at 60° – 70° S, and these signals extend downward into the upper troposphere and lower stratosphere, leading to a weak equatorward shift of the tropospheric jet (Fig. 4i). Moreover, synoptic waves shift the tropospheric jet poleward, with a deep acceleration on the jet's poleward flank from the surface to the stratosphere (Fig. 4l). This deep acceleration (i.e., a stratospheric control from synoptic waves) was also reported in KP04, and it can be partly understood by the downward control theory as a barotropic zonal wind response above the level of the eddy forcing (Haynes et al. 1991). In addition, the zonal wind response to synoptic eddy forcing is partially canceled by the planetary eddy response in the troposphere and leaves a net poleward shift of the tropospheric jet, as observed in the full model (i.e., $FM_F - FM_C$).

What are the implications of the results above for our understanding of the tropospheric response to stratospheric ozone depletion–like cooling? If the DCWEF mechanism were the dominant mechanism at play, the equatorward jet shift associated with the planetary wave–induced residual circulations in Fig. 4i would be expected to be maintained or amplified by a positive synoptic eddy feedback. However, the stronger poleward tropospheric jet shift due to the synoptic eddy forcing in Fig. 4l suggests that the mechanism of DCWEF is not dominant.

To explicitly test the role of the synoptic eddy feedback, a synoptic wave model would be the first choice. Ideally, in the synoptic wave model, the planetary wave forcing due to ozone depletion–like cooling can be specified similarly to ZM_P , and these specified zonal flow anomalies represent the effects of downward control via altered residual circulation. Meanwhile, only the zonal-mean and the synoptic eddies are resolved in this synoptic wave model. This setup not only allows the synoptic eddy feedback to dominate in the troposphere

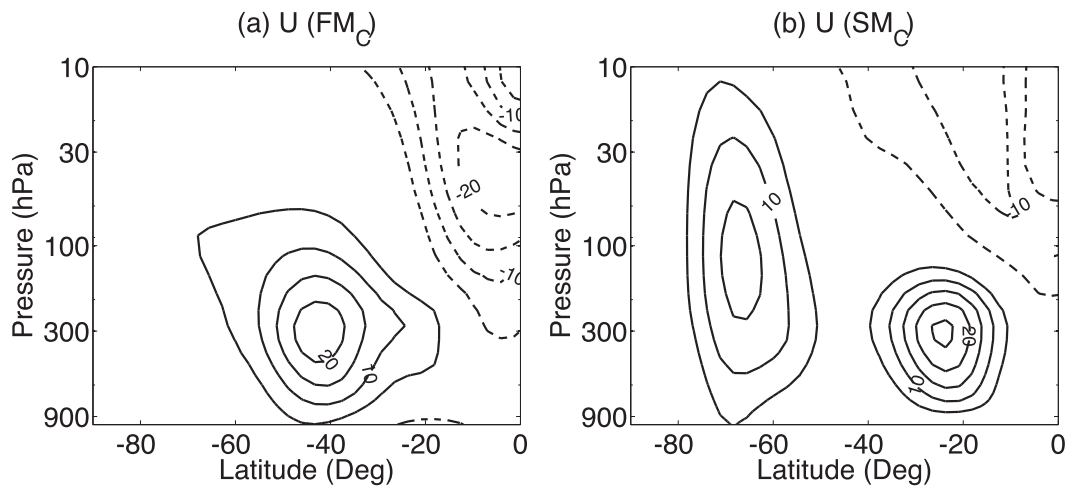


FIG. 5. Comparison on the climatology of zonal-mean zonal winds (m sec^{-1}) in (a) the full model (FM_C) and (b) the synoptic wave model (SM_C). See Table 1 for details. Implications of the results are as follows: keeping the zonal-mean planetary wave drags and resolving the synoptic eddies in SM_C produces a very different jet structure, as compared with FM_C . This indicates that the synoptic eddy–planetary eddy interaction (e.g., wave breaking) is crucial in maintaining the mean jet structure.

but also eliminates the nonlinear eddy–eddy interaction between planetary waves and synoptic waves. However, as shown in Fig. 5, the control run of this synoptic wave model (SM_C ; see Table 1 for details) is characterized with a double-jet structure, which is different from the single-jet structure in the full model (FM_C) and the zonally symmetric model (ZM_C). This indicates that the synoptic wave model is practically inappropriate for the explicit test of DCWEF in this current study. This also suggests that the nonlinear eddy–eddy interaction between planetary waves and synoptic waves, which is missing in SM_C , is critical to maintain the reasonable jet structure, despite a small contribution from planetary waves to the zonal-mean eddy forcing.

Instead, an additional experiment, denoted by FM_P in Table 1, is performed in the full model. In this

experiment, we specify anomalous zonal-mean planetary wave forcing extracted as the difference between the perturbed run and the control run, $\text{FM}_F - \text{FM}_C$. Compared with the full model simulation in FM_F , only the zonal-mean forcings of anomalous planetary eddies are included in this experiment, and therefore the majority of the eddy–eddy interactions with planetary waves are excluded. Note that the resolved planetary waves in FM_P can also be affected by the specified zonal-mean planetary wave forcing (i.e., $\text{FM}_F - \text{FM}_C$). This limitation counts as an important factor to explain the simulated stratospheric zonal wind difference between FM_F and FM_P (cf. Figs. 3f and 6c). In comparison with the corresponding zonally symmetric model simulation in ZM_P , the specified anomalous planetary wave forcing is identical, but the synoptic eddy feedback is allowed in

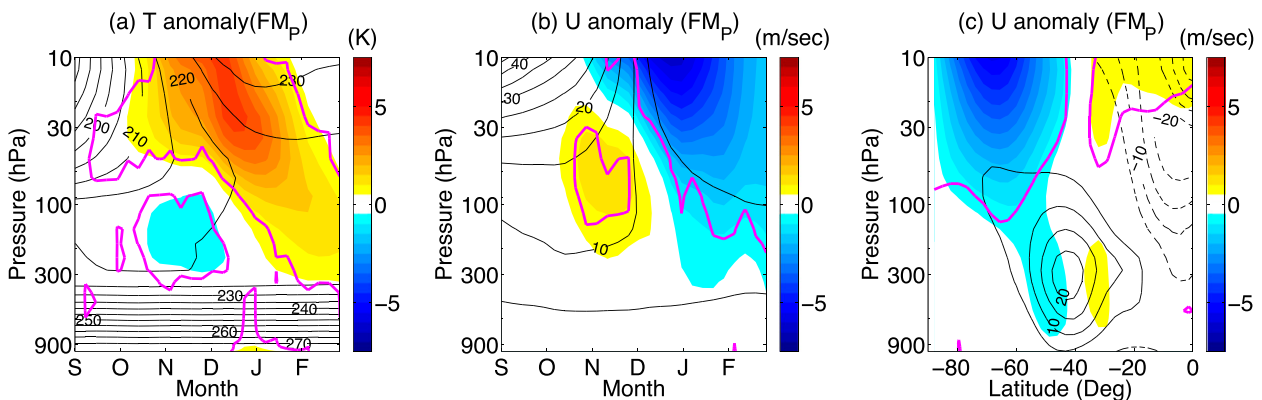


FIG. 6. As in Fig. 3d–f, but for specified anomalous zonal-mean planetary wave forcing extracted as the difference between the perturbed run (with ozone depletion–like cooling) and the control run in the full model (i.e., $\text{FM}_F - \text{FM}_C$). See the text in section 4 for details.

FM_p. Therefore, this can be approximately thought of as a direct simulation of the DCWEF response to the anomalous planetary wave drag induced by ozone depletion–like radiative cooling.

The results are displayed in Fig. 6. Generally speaking, the response to anomalous planetary wave forcing in the full model resembles its counterpart in the zonally symmetric model (cf. Figs. 6a–c and 4g–i), except for the meridional structure of the DJF stratospheric zonal wind anomaly seen in Fig. 6c. This is not surprising, as these stratospheric changes are primarily driven by specified anomalous planetary wave drag. Moreover, even in the presence of synoptic eddy feedbacks, the anomalous planetary eddy forcing produces a weak equatorward shift in the tropospheric jet (cf. Fig. 6c), in contrast to the poleward movement of the tropospheric jet in response to polar stratospheric cooling in the full model (cf. Fig. 3f). Therefore, this directly supports that DCWEF is not the dominant mechanism in generating the poleward tropospheric jet shift in response to stratospheric ozone depletion–like cooling in this full model. This is consistent with the implication deduced from Figs. 4i and 4l, characterized with opposite tropospheric jet shifts under the influences of planetary waves versus synoptic waves.

As noted in section 1, Sun et al. (2014) found that only the composite from the years with delayed SFW has a prominent tropospheric circulation response. The tropospheric response associated with the delayed SFW could be attributed to either an anomalous temperature cooling in the lowermost stratosphere (see their Fig. 10) that impacts synoptic eddies directly (i.e., the first mechanism in Fig. 1a) or the changes in the planetary eddies (see their Fig. 11) that further influence the synoptic eddies via nonlinear eddy–eddy interaction (i.e., the third mechanism in Fig. 1c). However, given that the stratospheric cooling tends to propagate upward in the summer by only imposing the radiative forcing with eddies being fixed, as shown in Fig. 4d, we argue that the summertime temperature cooling in the lowermost stratosphere [compare with Fig. 3d, similar to Fig. 10 in Sun et al. (2014)] is unlikely to be caused by a pure downward advection of the imposed radiative cooling but rather with the aid of altered eddies (cf. Figs. 4g,j).

Therefore, we propose that the tropospheric circulation response is less likely to be contributed solely by a direct impact on the synoptic eddies from the imposed radiative perturbation. A synthetic influence from both the imposed radiative cooling and resultant planetary wave changes onto the synoptic eddies in the upper troposphere and lower stratosphere that triggers the tropospheric circulation response remains possible in this model simulation, but the importance of eddies, in

particular the planetary eddies at the altitude of the imposed radiative cooling, seems to be crucial in the downward influence. To further confirm the dominance of the altered planetary eddies and subsequent nonlinear eddy–eddy interaction in Fig. 1c, one could investigate the planetary wave structure changes in response to the imposed perturbation, as in this mechanism, planetary waves can communicate between the stratosphere and troposphere by wave propagation (e.g., Chen and Robinson 1992) or reflection (e.g., Shaw et al. 2010).

5. Conclusions

We have examined transient atmospheric responses to stratospheric ozone depletion–like cooling in the idealized model of KP04. Despite its simplicity, the idealized model captures approximately the pattern and timing of the austral summertime circulation trends associated with radiative cooling (McLandress et al. 2010; Lin and Fu 2013; Thompson et al. 2011). In contrast to the unrealistic long persistence of the tropospheric response in KP04, the tropospheric persistence in our simulation is reasonable, as compared with observations. This was also noted by Kushner and Polvani (2006), who pointed out that the seasonal cycle of T_{eq} in the stratosphere helps to reduce the unrealistically long persistence in the tropospheric response seen in KP04.

By extending the method of KP04 and Domeisen et al. (2013) to different wavenumbers in the context of the seasonal cycle, we are able to separate the mechanisms of transient atmospheric responses to stratospheric radiative cooling in a zonally symmetric model. While the initial responses, mostly in the stratosphere, are caused by a direct adjustment to thermal forcing, the subsequent downward migration of signals is primarily driven by eddy forcing. We found that the synoptic eddies shift the tropospheric jet poleward, as in the full model with ozone depletion–like radiative cooling, against a weak equatorward tendency of the jet associated with the planetary wave forcing. This indicates that the equatorward tropospheric jet shift due to the planetary wave–induced residual circulations, arguably a result of stratospheric eddy–zonal flow interaction, is not maintained by a positive synoptic eddy feedback in the troposphere. This contrasts with the mechanism of planetary eddy–induced residual circulation in the tropospheric response to stratospheric forcing (Song and Robinson 2004; Thompson et al. 2006). However, the stratospheric forcing considered by Song and Robinson (2004) and Thompson et al. (2006) is associated with major stratospheric variability, rather than an external forcing like the stratospheric ozone depletion–like cooling imposed in this study.

Furthermore, the tropospheric circulation response associated with the polar stratospheric cooling, consistent with the delayed SFW composite in Sun et al. (2014), could be contributed from a direct impact from the imposed radiative perturbation to synoptic eddies in the upper troposphere and lower stratosphere, an indirect impact from the radiative perturbation via resultant planetary wave changes and subsequent nonlinear eddy–eddy interaction or a synthetic impact from both. However, the temperature decrease in the lowermost stratosphere, the key in the mechanism for a direct impact to the synoptic eddies, is unlikely to be a pure advection of the imposed radiative cooling from higher altitudes; the aids from altered eddies are critical. Therefore, this mechanism for a direct impact alone does not fully explain the downward influence of the polar stratospheric cooling toward tropospheric circulation response, and the role of the planetary eddies seem to be crucial. In this mechanism, resultant planetary wave changes from imposed radiative perturbation propagate from the stratosphere to the troposphere through wave propagation (e.g., Chen and Robinson 1992) or reflection (e.g., Shaw et al. 2010), which in turn impacts synoptic eddies through nonlinear eddy–eddy interactions.

While our simulations compare well with other studies with more sophisticated GCMs and realistic ozone depletion (McLandress et al. 2010; Orr et al. 2013), our results may be limited by the simplicity of the idealized model. One key simplification of the model is the flat lower boundary, which causes the planetary waves to be solely generated by nonlinear wave–wave interactions (Scinocca and Haynes 1998). In reality, planetary waves in the SH may be additionally generated by land–sea contrast or topography. This is partly reflected in that the zero-wind line in the summertime stratospheric wind is higher (or wave drag is weaker) in the idealized model, as compared with the observations (cf. Figs. 3c,f). Meanwhile, the onset date for the stratospheric final warming is generally too late in the current climate models (e.g., Wilcox and Charlton-Perez 2013). It would be interesting to explore the sensitivities of the dynamical mechanisms with respect to the model biases in the summer stratosphere relative to the observed climate.

Acknowledgments. We thank Walt Robinson for our discussions. We also thank three anonymous reviewers whose comments have led to substantial improvements of the manuscript. The authors are supported by the National Science Foundation (NSF) climate and large-scale dynamical program under Grant AGS-1042787. LS is also partly supported by the NSF Arctic sciences program.

APPENDIX

Calculation of the Annual Cycle of Eddy Forcings

We follow the method described in Domeisen et al. (2013) that extends the time-mean eddy forcing in KP04 to instantaneous eddy forcing and to zonal-wavenumber decomposition. The method can be illustrated using an advection equation with a damping term:

$$\frac{\partial q}{\partial t} = -\mathbf{u} \cdot \nabla q - k(q - q_{\text{eq}}) \equiv F(u, q), \quad (\text{A1})$$

where q is a tracer, k is a damping rate, and q_{eq} is a prescribed zonally symmetric equilibrium profile of the tracer. The term $F(u, q)$ is an operator for the instantaneous local tendency of q associated with advection and damping. We apply the tendency operator $F(\dots)$ to the zonal-mean terms:

$$\overline{F(\bar{u}, \bar{q})} = -\bar{u} \cdot \nabla \bar{q} - k(\bar{q} - q_{\text{eq}}) \quad (\text{A2})$$

and then to the zonal means plus an eddy component (e.g., synoptic, planetary, or total eddies)

$$\overline{F(\bar{u} + u^e, \bar{q} + q^e)} = -\bar{u} \cdot \nabla \bar{q} - k(\bar{q} - q_{\text{eq}}) - \overline{u^e \cdot \nabla q^e}. \quad (\text{A3})$$

Here, overbars denote the zonal means, and the superscript e denotes an eddy term. The eddy forcing can be obtained from the difference between Eqs. (A2) and (A3) to yield

$$\overline{u^e \cdot \nabla q^e} = \overline{F(\bar{u}, \bar{q})} - \overline{F(\bar{u} + u^e, \bar{q} + q^e)}. \quad (\text{A4})$$

In practice, the tendency operator is calculated by integrating the primitive equation model forward by one time step using instantaneous daily zonal and meridional winds, temperature, and surface pressure. We first calculate the tendencies for the zonal-mean fields and then compute the tendencies for zonal means plus the eddy term. The difference of the two yields the instantaneous eddy forcing in Eq. (A4). The annual cycle of the eddy forcing is obtained by averaging on the same day of all 80 years. The same procedure is repeated for synoptic, planetary, and total eddy forcings.

The zonally symmetric model, corresponding to the full model as described by Eq. (A1), is constructed as follows:

$$\frac{\partial \tilde{q}}{\partial t} = -\tilde{u} \cdot \nabla \tilde{q} - k(\tilde{q} - q_{\text{eq}}) - \overline{u^s \cdot \nabla q^s} - \overline{u^p \cdot \nabla q^p}, \quad (\text{A5})$$

where the model variables \tilde{q} and \tilde{u} are zonally symmetric (i.e., only the zonal means are resolved and integrated

forward in the model). The synoptic eddy forcing $-u^s \cdot \nabla q^s$ and planetary eddy forcing $-u^p \cdot \nabla q^p$ are derived from the corresponding full model by Eq. (A4), and then these eddy forcings are specified in the zonally symmetric model. More explicit expressions of the zonally symmetric model with zonal winds, temperature, and surface pressure can be found in appendix B of Sun et al. (2011). As shown by a comparison between Figs. 3d–f and 4a–c, the zonally symmetric model simulation successfully reproduces the full model responses to polar stratospheric cooling.

REFERENCES

- Andrews, D. G., J. R. Holton, and C. B. Leovy, 1987: *Middle Atmosphere Dynamics*. International Geophysics Series, Vol. 40, Academic Press, 489 pp.
- Butler, A. H., D. W. J. Thompson, and R. Heikes, 2010: The steady-state atmospheric circulation response to climate change–like thermal forcings in a simple general circulation model. *J. Climate*, **23**, 3474–3496, doi:10.1175/2010JCLI3228.1.
- Chen, G., and I. M. Held, 2007: Phase speed spectra and the recent poleward shift of Southern Hemisphere surface westerlies. *Geophys. Res. Lett.*, **34**, L21805, doi:10.1029/2007GL031200.
- , and L. Sun, 2011: Mechanisms of the tropical upwelling branch of the Brewer–Dobson circulation: The role of extratropical waves. *J. Atmos. Sci.*, **68**, 2878–2892, doi:10.1175/JAS-D-11-044.1.
- Chen, P., and W. Robinson, 1992: Propagation of planetary waves between the troposphere and stratosphere. *J. Atmos. Sci.*, **49**, 2533–2545, doi:10.1175/1520-0469(1992)049<2533:POPWBT>2.0.CO;2.
- Dee, D. P., and Coauthors, 2011: The ERA-Interim reanalysis: Configuration and performance of the data assimilation system. *Quart. J. Roy. Meteor. Soc.*, **137**, 553–597, doi:10.1002/qj.828.
- Domeisen, D. I. V., L. Sun, and G. Chen, 2013: The role of synoptic eddies in the tropospheric response to stratospheric variability. *Geophys. Res. Lett.*, **40**, 4933–4937, doi:10.1002/grl.50943.
- Haynes, P. H., and T. G. Shepherd, 1989: The importance of surface pressure changes in the response of the atmosphere to zonally symmetric thermal and mechanical forcing. *Quart. J. Roy. Meteor. Soc.*, **115**, 1181–1208, doi:10.1002/qj.49711549002.
- , C. J. Marks, M. E. McIntyre, T. G. Shepherd, and K. P. Shine, 1991: On the “downward control” of extratropical diabatic circulation by eddy-induced mean zonal forces. *J. Atmos. Sci.*, **48**, 651–678, doi:10.1175/1520-0469(1991)048<0651:OTCOED>2.0.CO;2.
- Kushner, P., and L. Polvani, 2004: Stratosphere–troposphere coupling in a relatively simple AGCM: The role of eddies. *J. Climate*, **17**, 629–639, doi:10.1175/1520-0442(2004)017<0629:SCIARS>2.0.CO;2.
- , and —, 2006: Stratosphere–troposphere coupling in a relatively simple AGCM: Impact of the seasonal cycle. *J. Climate*, **19**, 5721–5727, doi:10.1175/JCLI4007.1.
- Lin, P., and Q. Fu, 2013: Changes in various branches of the Brewer–Dobson circulation from an ensemble of chemistry climate models. *J. Geophys. Res. Atmos.*, **118**, 73–84, doi:10.1029/2012JD018813.
- Lorenz, D. J., and D. L. Hartmann, 2001: Eddy–zonal flow feedback in the Southern Hemisphere. *J. Atmos. Sci.*, **58**, 3312–3327, doi:10.1175/1520-0469(2001)058<3312:EZZFIT>2.0.CO;2.
- , and E. T. DeWeaver, 2007: Tropopause height and zonal wind response to global warming in the IPCC scenario integrations. *J. Geophys. Res.*, **112**, D10119, doi:10.1029/2006JD008087.
- McLandsess, C., A. I. Jonsson, D. A. Plummer, M. C. Reader, J. F. Scinocca, and T. G. Shepherd, 2010: Separating the dynamical effects of climate change and ozone depletion. Part I: Southern Hemisphere stratosphere. *J. Climate*, **23**, 5002–5020, doi:10.1175/2010JCLI3586.1.
- Orr, A., T. J. Bracegirdle, J. S. Hosking, T. Jung, J. D. Haigh, T. Phillips, and W. Feng, 2012: Possible dynamical mechanisms for Southern Hemisphere climate change due to the ozone hole. *J. Atmos. Sci.*, **69**, 2917–2932, doi:10.1175/JAS-D-11-0210.1.
- , —, —, W. Feng, H. K. Roscoe, and J. D. Haigh, 2013: Strong dynamical modulation of the cooling of the polar stratosphere associated with the Antarctic ozone hole. *J. Climate*, **26**, 662–668, doi:10.1175/JCLI-D-12-00480.1.
- Polvani, L. M., D. W. Waugh, G. J. P. Correa, and S.-W. Son, 2011: Stratospheric ozone depletion: The main driver of twentieth-century atmospheric circulation changes in the Southern Hemisphere. *J. Climate*, **24**, 795–812, doi:10.1175/2010JCLI3772.1.
- Scinocca, J. F., and P. H. Haynes, 1998: Dynamical forcing of stratospheric planetary waves by tropospheric baroclinic eddies. *J. Atmos. Sci.*, **55**, 2361–2392, doi:10.1175/1520-0469(1998)055<2361:DFOSPW>2.0.CO;2.
- Shaw, T. A., J. Perlwitz, and N. Harnik, 2010: Downward wave coupling between the stratosphere and troposphere: The importance of meridional wave guiding and comparison with zonal-mean coupling. *J. Climate*, **23**, 6365–6381, doi:10.1175/2010JCLI3804.1.
- Simpson, I. R., M. Blackburn, and J. D. Haigh, 2009: The role of eddies in driving the tropospheric response to stratospheric heating perturbations. *J. Atmos. Sci.*, **66**, 1347–1365, doi:10.1175/2008JAS2758.1.
- Song, Y., and W. A. Robinson, 2004: Dynamical mechanisms for stratospheric influences on the troposphere. *J. Atmos. Sci.*, **61**, 1711–1725, doi:10.1175/1520-0469(2004)061<1711:DMFSIO>2.0.CO;2.
- Sun, L., and W. A. Robinson, 2009: Downward influence of stratospheric final warming events in an idealized model. *Geophys. Res. Lett.*, **36**, L03819, doi:10.1029/2008GL036624.
- , —, and G. Chen, 2011: The role of planetary waves in the downward influence of stratospheric final warming events. *J. Atmos. Sci.*, **68**, 2826–2843, doi:10.1175/JAS-D-11-014.1.
- , G. Chen, and W. A. Robinson, 2014: The role of stratospheric polar vortex breakdown in Southern Hemisphere climate trends. *J. Atmos. Sci.*, **71**, 2335–2353, doi:10.1175/JAS-D-13-0290.1.
- Thompson, D. W. J., J. C. Furtado, and T. G. Shepherd, 2006: On the tropospheric response to anomalous stratospheric wave drag and radiative heating. *J. Atmos. Sci.*, **63**, 2616–2629, doi:10.1175/JAS3771.1.
- , S. Solomon, P. J. Kushner, M. H. England, K. M. Grise, and D. J. Karoly, 2011: Signatures of the Antarctic ozone hole in Southern Hemisphere surface climate change. *Nat. Geosci.*, **4**, 741–749, doi:10.1038/ngeo1296.
- Wilcox, L. J., and A. J. Charlton-Perez, 2013: Final warming of the Southern Hemisphere polar vortex in high- and low-top CMIP5 models. *J. Geophys. Res. Atmos.*, **118**, 2535–2546, doi:10.1002/jgrd.50254.
- Williams, G. P., 2006: Circulation sensitivity to tropopause height. *J. Atmos. Sci.*, **63**, 1954–1961, doi:10.1175/JAS3762.1.
- Wittman, M. A. H., A. J. Charlton, and L. M. Polvani, 2007: The effect of lower stratospheric shear on baroclinic instability. *J. Atmos. Sci.*, **64**, 479–496, doi:10.1175/JAS3828.1.